COMMUNICATIONS IN COMPUTATIONAL PHYSICS
Vol. **6**, No. 4, pp. 699-729

Commun. Comput. Phys.
October 2009

Spurious Solutions in the Multiband Effective Mass Theory Applied to Low Dimensional Nanostructures

B. Lassen[1], R. V. N. Melnik[2,*] and M. Willatzen[1]

[1] *The Mads Clausen Institute, The University of Southern Denmark, Alsion 2, DK-6400, Sonderborg, Denmark.*
[2] M^{2}NeT *Lab and Department of Mathematics, Wilfrid Laurier University, 75 University Avenue West, Waterloo, Ontario N2L 3C5, Canada.*

Received 21 September 2008; Accepted (in revised version) 5 January 2009

Communicated by Michel A. Van Hove

Available online 5 March 2009

Abstract. In this paper we analyze a long standing problem of the appearance of spurious, non-physical solutions arising in the application of the effective mass theory to low dimensional nanostructures. The theory results in a system of coupled eigenvalue PDEs that is usually supplemented by interface boundary conditions that can be derived from a variational formulation of the problem. We analyze such a system for the envelope functions and show that a failure to restrict their Fourier expansion coefficients to small k components would lead to the appearance of non-physical solutions. We survey the existing methodologies to eliminate this difficulty and propose a simple and effective solution. This solution is demonstrated on an example of a two-band model for both bulk materials and low-dimensional nanostructures. Finally, based on the above requirement of small k, we derive a model for nanostructures with cylindrical symmetry and apply the developed model to the analysis of quantum dots using an eight-band model.

AMS subject classifications: 35Q40, 81Q05, 65N25, 47N50, 33F05

PACS: 73.21.La, 73.22.Dj, 71.15.-m, 02.30.-f, 02.70.-c

Key words: Effective envelope theory, quantum confinement, abrupt interfaces, multiband models, k space, Fourier coefficients, highly oscillatory integrals, variational formulation, coupled systems of PDEs, multiple scales, continuum and atomistic models, eigenvalue problem, interface boundary conditions, band gap, spurious solutions, low dimensional semiconductor nanostructures.

*Corresponding author. *Email addresses:* benny@mci.sdu.dk (B. Lassen), rmelnik@wlu.ca (R. V. N. Melnik, http://www.m2netlab.wlu.ca), willatzen@mci.sdu.dk (M. Willatzen)

1 Introduction

The electronic structure calculation is among the most fundamental problems in modern science and engineering. While achieving a higher accuracy in the methods for such calculations remains an important issue, our ability to construct simpler computational algorithms that would allow us to obtain reliable results in a more efficient and cost-effective manner is paramount for our progress at the practical level with far reaching ramifications in technological applications.

From a mathematical point of view, most methodologies for the construction of such algorithms are based on effective theories where we attempt to reduce the degrees of freedom and to bridge modelling scales [58, 67]. One such theory, derived with the application of the effective mass theorem [84] and known as the multiband effective mass approximation, provides a fundamental tool in predicting electronic properties of structures. We are interested in the development of an efficient computational tool for predicting electronic properties of quantum heterostructures, that is the low-dimensional (semiconductor) nanostructures where the motion of electrons is restricted, forcing them into a quantum confinement [33–35, 100]. Examples of such structures include quantum wells, quantum wires, or quantum dots, where the motion of electrons is restricted in one, two, or all three directions, respectively. Properties of these small nanocrystals, containing often from a few hundred to a few thousand atoms, are very different from the same material in bulk, which results in a wide range of their current and potential applications, from biological tags for proteins to applications in quantum computing, and to a new generation of optoelectronic devices [63, 65, 66].

The reason for our undertaking stems from the fact that typical characteristic dimensions of nanostructures is ranging between 1 to 100 nm while the characteristic dimensions of atoms are between 0.1 to 0.7nm. Over the last decade, a substantial progress in the development of atomistic methodologies for handling such structures (including the device level) has been achieved and we discuss some of the major highlights of this development in Section 2.2. However, it is widely understood in the research community that in many practical situations atomistic approaches remain computationally prohibitive and the development of simple, often continuum-based, mathematical models and their efficient computational implementations become very important. This is particularly true when we have to account for a multiscale nature of the problem (e.g., [28, 59, 61, 64, 67]) and its multiphysics character where several physical fields, such as mechanical, electric, and/or thermal act simultaneously and we have to deal with coupled problems (e.g., [29, 40–43, 49–58, 75, 76, 82, 83, 90–94, 101]).

Coupled problems arise frequently in the applications to nanoscience and nanotechnology and they bring new challenges at the level of the development of mathematical models and efficient numerical methodologies for their solution. Such problems are intrinsic to the multiband effective mass theory, a major focus of the present paper. In dealing with (nano)crystals we use the fact of crystal symmetry characterized by the transformations which in the bulk case leave the structure, and hence its Hamiltonian

(the energy operator), invariant. The representations of the translation group are characterized by a vector **k** in the first Brillouin zone of the crystal. The relevance of the **k** vector is clearly seen from the Bloch theorem, stating that any solution for a periodic structure (bulk material) can be represented in the form:

$$\psi_{n\mathbf{k}}(\mathbf{r}) = \exp(i\mathbf{kr})u_{n,\mathbf{k}}(\mathbf{r}), \tag{1.1}$$

where $u_{n,\mathbf{k}}$ has the given periodicity. The n in Eq. (1.1) reflects a multiband nature of the energy operator spectrum and the basic task in the **k**-space can be formulated as the determination of this spectrum throughout one Brillouin zone (usually, the first Brillouin zone). In the case of a nanocrystal this theorem does not apply anymore. Instead, the wave function can be expanded in terms of Bloch solutions:

$$\psi(\mathbf{r}) = \sum_n \int c_n(\mathbf{k}) \exp(i\mathbf{kr}) u_{n,\mathbf{k}}(\mathbf{r}) d^3k, \tag{1.2}$$

where the integral is over the first Brillouin zone. It turns out that it is advantageous to rewrite the expansion in term of a specific set of periodic solutions, and the zone-center solutions $u_{n,0}$ are usually chosen for this purpose. Hence, by using $u_{n,\mathbf{k}}(\mathbf{r}) = \sum_{n'} d_{nn'}(\mathbf{k}) u_{n',0}(\mathbf{r})$, we get:

$$\psi(\mathbf{r}) = \sum_n \int \tilde{F}_n(\mathbf{k}) \exp(i\mathbf{kr}) d^3k u_{n,0}(\mathbf{r}) = \sum_n F_n(\mathbf{r}) u_{n,0}(\mathbf{r}), \tag{1.3}$$

where $\tilde{F}_n(\mathbf{k}) = \sum_{n'} c_{n'}(\mathbf{k}) d_{n'n}(\mathbf{k})$. The idea of the envelope function (EF) based on the representation (1.3) is a key to a substantial simplification of the original problem in determining properties of the heterostructures. This representation leads to a major advantage of the EF multiband effective mass methodologies compared to computationally intensive ab initio and atomistic approaches and allows us to extend the energy-band theory beyond perfectly periodic crystals. Known for bulk materials since 50-ies (e.g., [2,10,39,81]), this methodology has successfully been extended to situations that allow us to treat efficiently lattice-mismatched heterostructures where we frequently have to deal with two (or more) materials with different properties, both theoretically and computationally [4–6, 12, 27]. One of the main difficulties in implementing multiband effective mass models is the appearance of spurious solutions. Although these solutions are correct solutions of the multiband model in question, they have nothing to do with the physics of the problem as they are not solutions to the original problem (e.g., [30,31]).

The goal of this paper is twofold. First, we want to highlight the reason for the appearance of spurious solutions using a simple one dimensional two band model and give an overview of different approaches for the removal of spurious solutions. Second, within one of the approaches, the so-called cut-off method, we show how additional symmetries can be taken into account. More specifically, we show how a three dimensional cylindrical symmetric problem can be simplified and demonstrate the effectiveness of the developed multiband model in applications to quantum dots.

The structure of the rest of the paper is as follows. In the next section we explain the main difficulties in applying the effective mass theory to the analysis of nanostructures and provide an overview of existing methodologies directed to the elimination of spurious solutions. In this section we also provide the reader with a discussion of the main approaches in this field to the treatment of interface boundary conditions not only in the context of effective mass $\mathbf{k}\cdot\mathbf{p}$ theory, but also for other computationally promising methods. In Section 3 we give details of the basic model obtained from the generalized envelope function theory in one dimension, followed by two examples. The first example is concerned with a stepwise constant crystal potential and deal with the bulk situation. The second example is concerned with the treatment of a heterostructure where we have to deal with abrupt interface conditions. This example demonstrates difficulties in the application of the envelope function theory in practice, connected with the spurious solution phenomenon. We highlight the physical roots of this problem and a computational procedure to circumvent arising difficulties. In Section 4 we demonstrate this procedure on an example of cylindrically symmetric systems. The developed multiband model is applied to the analysis of symmetric quantum dot nanostructures. Conclusions and future directions are presented in Section 5.

2 Interface boundary conditions, spurious solutions, and existing methodologies

As a framework for the discussion we show in Fig. 1 a schematic representation of a nanoscale heterostructure.

2.1 Regularity of the envelope function

The first question that arises in the context of the model we are considering here is about the regularity of the envelope function at the interface (the abrupt heterojunction), in

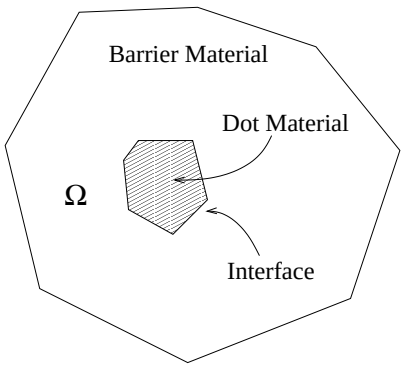

Figure 1: Schematic picture of a nanoscale heterostructure.

particular whether this function is continuous or discontinuous. If the Fourier components of the envelope function are clustered around the center of the interval where the problem is considered, then the model is reducible to the standard Sturm-Liouville eigenvalue problem for the second order differential operator. Otherwise, a higher order model needs to be considered. Connection rules (or the interface boundary conditions) are needed to link the solutions from two different regions at the interface. Such rules can be continuous and represented by certain phenomenological conditions with empirical coefficients that play the role of material parameters characterizing the interface [86] or discontinuous, in agreement with traditional concepts. In the first case, the regularity of the envelope function must be relaxed. In the second case, we usually use bulk properties for an extrapolation across the interface defining the connection rules which are in this case discontinuous with the interface width of the order of a lattice constant [14]. Both cases are physically equivalent. Furthermore, the envelope-function theory can be applied to the analysis of nanostructures even in the latter case [5, 7, 12]. According to this theory, the solution to the eigenvalue PDE problem

$$H\mathbf{F} = E\mathbf{F}, \tag{2.1}$$

with H being the effective mass Hamiltonian, can be represented in terms of momentum matrix elements and band gaps, including the interfaces. This is shown by deriving a set of integro-differential equations for envelope functions and restricting our attention to the behavior of such functions on the scale larger than the lattice constant by neglecting nonlocal terms. From an experimental point of view, even in the case of large lattice mismatches, many nanostructures, including nanowire heterostructures, exhibit defect-free interfaces [11], making such an assumption well justified. In the general case, the validity of such an approximation in a narrow region near the interface requires, strictly speaking, linking the proposed approach to atomistic methodologies (these ideas result in atomitic-to-continuum methods, see more in Section 2.3). Another approach, based on an averaging procedure around the interface and valid to the order of around 1Å (the distance between interface atoms) was proposed in [85]. It is important to emphasize here that the problem of formulating correct interface boundary conditions is not limited to the effective mass theory and is debated in the literature in the context of other models in the multiscale hierarchy of mathematical models for nanostructures, e.g. for pseudopotential-based models as well as for tight-binding models [32] and we provide more details on this issue in the next section.

As mentioned, the physical reason behind this debate is the fact that the internal structure of the heterointerface cannot be represented in terms of bulk parameters [86]. This fact and the required reparametrization due to necessary fittings to experimental data may lead to difficulties in the formulation of model (2.1) satisfying ellipticity properties [87]. On the other hand, it is exactly the internal structure of the heterointerface that leads to unique properties of such nanostructures and lend them wide applicability. Several recent approaches have been proposed to overcome the problem in the context of the effective mass theory based on additional requirements. For example, in [77] the authors

used the conservation property of probability density to derive boundary conditions for the envelope functions from the conservation of the current normal to the interface. The derivation of the variational principle for the effective mass theory model has recently been discussed in [78] where phenomenological parameters, in addition to the bulk parameters, are required for the implementation.

2.2 Beyond the k·p theory and boundary conditions

Despite the ever-increasing computational capabilities, the **k**·**p** method continues to serve as an important bandstructure tool and often so in combination with atomistic models for solving problems of quantum-confined heterostructures. As of today, more than 1500 papers appear in the literature employing **k**·**p** method arguments [36]. Some of the more recent applications to low-dimensional applications are related to spin-splitting investigations in Si/SiGe quantum-well systems accounting for Rashba-type contributions [69], computation of electromechanical field interactions in quantum-dot wetting-layer structures [37, 79], including nonlinear effects [58], and eight-band modelling of quantum-confined Stark effect in Ge quantum-well structures with implications for electro-optics [73], to name just a few.

Among other methodologies for bandstructure calculations, we have already mentioned here tight binding and empirical pseudopotential methods which often provide computationally moderate cost alternatives to the **k**·**p** approximations. Proposed by E. Fermi in early 1930s, the concept of pseudopotential has been developed to an important bandstructure tool. It is usually based on an (orthogonalized) plane wave expansion and, as a result, it is most suitable for periodic structures where periodic boundary conditions are assumed. A substantial improvement was introduced in [95] where a "linear combination of bulk bands" method was developed. Although the method still requires periodic supercell conditions in all spatial dimensions, it leads to a substantial computational speed-up compared to the conventional plane-wave methodologies, allowing to deal with million atom nanostructures. Other more recent modifications that have further advantages over the conventional plane-wave-based pseudopotentials for bandstructure calculations include real-space methodologies [21]. They are often based on local numerical discretizations such as finite differences [70], applied widely for bandstructure calculations of low dimensional nanostructures [19], and periodic boundary conditions are not necessary for their implementations [22,71]. First principles and DFT based methods that use pseudopotentials have been applied for both bandstructure calculations and the analysis of properties of nanostructures [1,71,96,97]. The pros and cons of these more refined methodologies have been recently highlighted in [23].

The application of tight-binding methods is computationally quite efficient in the case of periodic (cyclic) boundary conditions [44], but in the general case the formulation of boundary conditions is usually a compromise between the accuracy and convergence properties of the developed method [32, 38].

Boundary conditions for multiband envelope function approximations are not limited

to periodic. However, due to experimentally fitted parameters the ellipticity conditions for the corresponding coupled systems of PDEs may be violated, leading to spurious solutions and in the next section we highlight the main tools available to deal with this phenomenon.

2.3 Experimental effective masses and spurious solutions

An accurate fit to all experimental effective masses in the multi-band effective mass Hamiltonian H from model (2.1) may lead to spurious, non-physical solutions that contradict one of the most fundamental physical observations, the existence of a band gap in these semiconductor materials. It is a long standing problem known from the literature for quite some time [98]. If all solutions are retained, there are repeated arguments in the literature that spurious bands have a negligible effect on the bound-state eigenfunction properties. However, it has been shown that this methodology may lead to the results that contradict physical observations [13]. Recall that the premises of the effective mass theory lies with the fact that the model Hamiltonian is accurate in the vicinity of $k=0$. Therefore, the main ideas for eliminating spurious solutions should rely either

- on the manipulations with higher order terms in the Hamiltonian, modifying the model (e.g., by using k^2 terms as in [26]), or
- on rejecting the larger-k solutions as non-physical from the outset (as in [20]).

The first approach is not as easy to implement in practice as we might think. One reason for that lies with the fact that Hamiltonian modifications should remain invariant with respect to symmetry operations of the corresponding groups. In what follows, we base our discussion on the second approach.

Before proceeding further, we mention that for efficient practical implementations it is important also to choose a basis that is a good approximation to the Bloch waves of the bulk materials the nanostructure is made of. This can be achieved in several different ways. For example, we can use an averaging procedure around the interface valid to the order of the distance between interface atoms and maintain the continuity of the envelope function as we mentioned before [85]. Alternatively, we can keep the discontinuity across the interface, defining it via the connection rules, and choose an appropriate basis (by choosing appropriate transformation parameters) such that spurious non-physical solutions are eliminated [13, 15]. The latter methodology has several advantages. For example, the matrix of the resulting system of linear equations under this approach is sparse allowing an efficient computational implementation. This methodology requires an additional assumption on operator ordering in the Hamiltonian.

In its essence, the multi-band $\mathbf{k}\cdot\mathbf{p}$ approach, leading to coupled systems of eigenvalue PDEs problems, is a continuum approach which can be combined with atomistic methodologies for complete nanostructure descriptions. Several efficient numerical procedures for the coupling atomistic and continuum calculations have already been proposed in the literature [25, 72]. Note also that when we reduce the original eigenvalue PDE problem

such as (2.1) to an algebraic eigenvalue problem, several non-trivial numerical difficulties may arise along the way [48]. Now, starting from the multiband effective mass theory in one dimension, we develop and apply a methodology that allows us to overcome the spurious solution phenomenon in a simple and efficient manner. Our final result is the application of the developed multiband method to bandstructure calculations of cylindrical quantum dots.

3 Multiband effective mass theory in one dimension

Consider the eigenvalue PDE problem (2.1) for a one dimensional crystalline heterostructure described by the following Hamiltonian:

$$H=-\frac{\hbar^2}{2m}\frac{\partial^2}{\partial x^2}+V(x), \tag{3.1}$$

in some region $\Omega\subseteq\mathbb{R}$ (see Fig. 1), where m is the free electron mass, $\hbar=h/(2\pi)$, and h is Planck's constant. In this case, as we mentioned in the introductory part, we have to deal with a multiscale problem where the two length scales are the atomistic and the heterostructure scales. These scales are contained within the potential $V(x)$ (see Section 3.2 for an example). The idea behind k·p theory is to replace one of these length scales, namely the atomistic scale, with material specific parameters. In this paper we use the envelope function theory developed by Burt [5] to achieve this.

Following [4] we start by expanding the wave function ψ in a complete set of periodic and orthonormal functions U_n:

$$\psi=\sum_n F_n(x)U_n(x), \tag{3.2}$$

where

$$F_n(x)=\int_{-\pi/a}^{\pi/a}\tilde{F}_n(k)e^{ikx}dk, \tag{3.3}$$

and a is the length of the period. The completeness of the set U_n only relates to functions with the given periodicity. In effective mass theory the periodicity is usually given by the principal lattice cell (see Appendix) although this need not be the case. The Fourier expansion is restricted to the first Brillouin zone only because this ensures uniqueness of the envelope functions F_n as is seen from the expansion in periodic Bloch functions in Eq. (1.2) (the first Brillouin zone is in the one dimensional case given by the interval $]-\pi/a,\pi/a]$). The usual choice of basis is the zone-center solutions $u_{n,0}$ as indicated in Section 2. Based on this expansion the following infinite set of coupled differential equations can be derived for the envelope functions [4]:

$$-\frac{\hbar^2}{2m}\frac{\partial^2 F_n}{\partial x^2}(x)+\sum_{n'}\frac{-i\hbar}{m}p_{nn'}\frac{\partial F_{n'}}{\partial x}(x)+\sum_{n'}\int_\Omega H_{nn'}(x,x')F_n(x')dx'=EF_n(x), \tag{3.4}$$

where

$$p_{nn'} = -i\hbar \int_{\Omega_a} U_n^*(x) \frac{\partial U_{n'}}{\partial x}(x) dx, \tag{3.5}$$

$$H_{nn'}(x,x') = K_{nn'}\delta(x-x') + V_{nn'}(x,x'), \tag{3.6}$$

$$K_{nn'} = -\frac{\hbar^2}{2m} \int_{\Omega_a} U_n^*(x) \frac{\partial^2 U_{n'}}{\partial x^2}(x) dx, \tag{3.7}$$

$$V_{nn'}(x,x') = aU_n^*(x')V(x')U_{n'}(x')\Delta(x-x'), \tag{3.8}$$

$$\Delta(x) = \frac{1}{2\pi} \int_{-\pi/a}^{\pi/a} e^{ikx} dk. \tag{3.9}$$

Here Ω_a denotes the region of one period, e.g., $]0,a]$. It is worth noting that the non-local term (the last term on the left of Eq. (3.4)) is a direct consequence of the first Brillouin zone cut-off. This is most easily seen by writing the set of equations in k-space instead of real space:

$$\frac{\hbar^2}{2m}k^2\tilde{F}_n(k) + \sum_{n'} \frac{\hbar}{m} p_{nn'} k \tilde{F}_{n'}(k) + \sum_{n'} \int_{-\pi/a}^{\pi/a} \tilde{H}_{nn'}(k-k')\tilde{F}_n(k')dk' = E\tilde{F}_n(k), \tag{3.10}$$

where

$$\tilde{H}_{nn'}(k-k') = K_{nn'}\delta(k-k') + \frac{a}{2\pi} \int_{\Omega} U_n^*(x)V(x)U_{n'}(x)e^{-i(k-k')x} dx. \tag{3.11}$$

If the integral in the third term on the left of Eq. (3.10) was not restricted to the first Brillouin zone the equations would be local in real space.

Either of these infinite sets of equations (Eq. (3.4) or Eq. (3.10)) can not be solved in general so we need to reduce the infinite set to a finite set of equations. This can in principle be achieved by finding a unitary operator W which block diagonalizes the problem. To be more specific, let us write Eq. (3.10) in a slightly different form:

$$\int_{-\pi/a}^{\pi/a} \hat{H}_{nn'}(k,k')\tilde{F}_{n'}(k')dk' = E\tilde{F}_n(k), \tag{3.12}$$

where

$$\hat{H}_{nn'}(k,k') = \left[\frac{\hbar^2}{2m}k^2\delta_{nn'} + \frac{\hbar}{m}p_{nn'}k\right]\delta(k-k') + \tilde{H}_{nn'}(k-k'). \tag{3.13}$$

We now divide the set U_n into two groups, a finite group denoted A which we want to solve for, and the rest we denote with R, these are called remote bands. We want to find a unitary operator W so that $\overline{H}_{nn'}(k,k') = [W^\dagger \hat{H} W]_{nn'}(k,k') = 0$ for all k,k' whenever $U_n \in A$ and $U_{n'} \in R$, where operator multiplication is given by:

$$[MN]_{nn'}(k,k') = \sum_l \int_{-\pi/a}^{\pi/a} M_{nl}(k,k'')N_{ln'}(k'',k')dk''. \tag{3.14}$$

We assume that $[MN]_{nn'}(k,k') < \infty$ for all n,n' and k,k'. In Section 3.2 we give an example where this requirement is easily seen to be fulfilled. Under the assumption that such a unitary matrix W exists we can reduce the problem to a finite set of equations. Although in the general case it is impossible to find W, this procedure suggests an approximation scheme. We first write W in terms of an operator S given so that $W = e^S$. We then expand S in terms of a power series with respect to a part of $\hat{H}$ assumed to be small. More specifically, we split $\hat{H}$ into two parts, a part assumed to be the main part of $\hat{H}$:

$$\hat{H}^0_{nn'}(k,k') = \tilde{H}_{nn}(0)\delta_{nn'}\delta(k-k'), \tag{3.15}$$

and the rest $\hat{H}^1_{nn'}(k,k') = \hat{H}_{nn'}(k,k') - \hat{H}^0_{nn'}(k,k')$, which is assumed to be small compared to $\hat{H}_0$. For each specific application it is important to verify that $\hat{H}^1$ is indeed small compared to $\hat{H}^0$. This turns out to be the root of the problem with spurious solutions. We will come back to this in Section 3.2. Now, we make an expansion around the center of the first Brillouin zone and write S as:

$$S = S^1 + S^2 + S^3 + \cdots, \tag{3.16}$$

where S^i is the term of order i with respect to elements of $\hat{H}^1$. Using

$$e^{-S}He^S = H + [H,S] + \frac{1}{2}[[H,S],S] + \cdots, \tag{3.17}$$

we can write $\overline{H}$ in terms of S^i collecting terms of a given order in $\hat{H}^1$, e.g., to the second order in $\hat{H}^1$:

$$\overline{H} = \hat{H}^0 + \hat{H}^1 + [\hat{H}^0,S^1] + [\hat{H}^1,S^1] + [\hat{H}^0,S^2] + \frac{1}{2}[[\hat{H}^0,S^1],S^1] + \cdots. \tag{3.18}$$

We can now choose S^1 so that $\overline{H}$ is block diagonal to the second order in $\hat{H}^1$, i.e., we choose S^1 so that:

$$[\hat{H}^0,S^1]_{nn'} = -\hat{H}^1_{nn'}, \tag{3.19}$$

for $U_n \in A$ and $U_{n'} \in R$, i.e.,

$$S^1_{nn'}(k,k') = \begin{cases} \frac{\hat{H}^1_{nn'}(k,k')}{\tilde{H}_{n'n'}(0) - \tilde{H}_{nn}(0)}, & \text{for } U_n \in A \text{ and } U_{n'} \in R, \\ 0, & \text{else.} \end{cases} \tag{3.20}$$

We then choose S^2 so that $\overline{H}$ is block diagonal to the third order in $\hat{H}^1$ and so on. Using this procedure we can reduce the problem to the finite set A to any order in $\hat{H}^1$. It is usual to disregard terms of third and higher orders in $\hat{H}^1$ resulting in the following set of equations:

$$\begin{aligned} \overline{H}_{nn'}(k,k') = &\left[\frac{\hbar^2}{2m}k^2\delta_{nn'} + \frac{\hbar}{m}p_{nn'}k\right]\delta(k-k') + \tilde{H}_{nn'}(k-k') \\ &+ \frac{1}{2}\sum_{r\in R}\left(\frac{1}{\tilde{H}_{nn}(0) - \tilde{H}_{rr}(0)} + \frac{1}{\tilde{H}_{n'n'}(0) - \tilde{H}_{rr}(0)}\right)\int_{-\pi/a}^{\pi/a}\hat{H}^1_{nr}(k,k'')\hat{H}^1_{rn}(k'',k')dk'', \end{aligned} \tag{3.21}$$

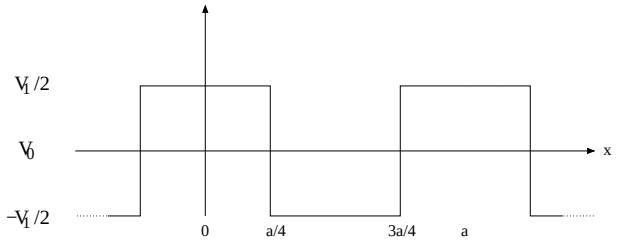

Figure 2: Bulk potential.

for $U_n, U_{n'} \in A$, where $r \in R$ stands for $U_r \in R$. These types of equations are called multiband equations although they are usually formulated in the form of PDEs, see Section 3.2.

Our final remark here is due to the fact that for problems like ours, we often have to deal with highly oscillatory integrals. For example, such integrals may arise in the context of Bessel functions factored in the integrands (see Section 4). Efficient numerical methodologies for dealing with such highly oscillatory integrals are available in the literature in both one-dimensional and multi-dimensional cases [24, 45–47, 103, 105].

We will now give two examples of the application of the theory presented in this section. In the first example we study bulk properties, i.e., we study the simple situation where the potential is periodic. This serves as a good test example for the application of mulitband equations as the results can be compared to exact (semi-analytical) solutions. It also serves as a framework for more difficult problems with heterostructures. In the second example we investigate a heterostructure for the explicit purpose of showing why spurious solutions appear. We also provide an example of how such spurious solutions can be removed.

3.1 Stepwise constant crystal potential in the bulk case

Let us first consider the case where we have a completely periodic potential $V(x)$ given by a stepwise constant potential (Fig. 2):

$$V(x) = V_0 + V_1\theta(x), \tag{3.22}$$

where

$$\theta(x) = \begin{cases} -\frac{1}{2} & \text{for } \frac{a}{4} < x < \frac{3a}{4}, \\ \frac{1}{2} & \text{else,} \end{cases} \tag{3.23}$$

for $x \in [0,a]$ and then repeated throughout $\mathbb{R}$, i.e., in this example $\Omega = \mathbb{R}$. The problem can in this case be solved semi-analytically in the sense that the solutions are given by zeros of a transcendental function. The exact solutions are found by using Bloch's theorem which in this case states that solutions are given by $e^{ikx}u_{n,k}(x)$ where $u_{n,k}(x)$ are periodic solutions to the equation:

$$-\frac{\hbar^2}{2m}\frac{\partial^2 u_{n,k}}{\partial x^2}(x) - \frac{i\hbar^2}{m}k\frac{\partial u_{n,k}}{\partial x}(x) + \frac{\hbar^2}{2m}k^2 u_{n,k} + V(x)u_{k,n}(x) = E_{n,k}u_{n,k}, \tag{3.24}$$

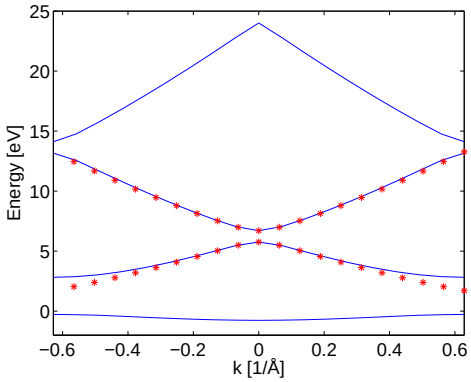

Figure 3: The solid lines show the three first exact dispersion curves and the dots show the dispersion curves found using the two band model. All results are with $V_0=0$ eV, $V=5$ eV and $a=5$ Å.

the index n is an integer and k is a continuous parameter. This equation can easily be solved by setting up a set of linear equations for the coefficients of the general solutions $e^{\pm ik_i x}$ in each region with constant potential resulting in a transcendental equation for the energies $E_{n,k}$. In Fig. 3 we show the band structure for a specific example, i.e., a plot showing eigen energies as a function of k.

Although we can easily find the exact solutions to this problem, there is still a lot to be learned by applying the above method. In the case of a periodic potential Eq. (3.11) reduces to:

$$\tilde{H}_{nn'}(k-k')=\delta(k-k')\int_0^a U_n^*(x)HU_{n'}(x)dx. \tag{3.25}$$

This suggests that periodic zone center eigen solutions to H will be a good choice for the periodic basis, i.e., $U_n=u_{n,0}$. With this choice $\tilde{H}_{nn'}(k,k')$ is diagonal and the diagonal elements are given by the periodic eigen energies, i.e.,

$$\tilde{H}_{nn'}(k-k')=E_{n,0}\delta_{nn'}\delta(k-k'), \tag{3.26}$$

and

$$\hat{H}^1_{nn'}(k,k')=\left[\frac{\hbar^2}{2m}k^2\delta_{nn'}+\frac{\hbar}{m}p_{nn'}k\right]\delta(k-k'). \tag{3.27}$$

It is clear from this that the elements of $\hat{H}^1_{nn'}$ will be small as long as k is small. In the general case, the question of how small is a currently unresolved non trivial issue. A rule of thumb is that k should be within the first 20% of the first Brillouin zone. Using Eq. (3.27), the multiband equation Eq. (3.21) takes on the simple form:

$$\overline{H}_{nn'}(k,k')=\left[\frac{\hbar^2}{2m}\gamma_{nn'}k^2+\frac{\hbar}{m}p_{nn'}k+E_{n,0}\delta_{nn'}\right]\delta(k-k'), \tag{3.28}$$

where

$$\gamma_{nn'}=\delta_{nn'}+\frac{1}{m}\sum_{r\in R}p_{nr}p_{rn}\left(\frac{1}{E_{n,0}-E_{r,0}}+\frac{1}{E_{n',0}-E_{r,0}}\right). \tag{3.29}$$

If we choose the second and third zone center solutions, i.e., $U_2 = u_{2,0}$ and $U_3 = u_{3,0}$ from Eq. (3.24), as our set A we get:

$$\begin{pmatrix} \frac{\hbar^2}{2m}\gamma_{22}k^2 + E_{2,0} & \frac{\hbar}{m}p_{23}k \\ \frac{\hbar}{m}p_{32}k & \frac{\hbar^2}{2m}\gamma_{33}k^2 + E_{3,0} \end{pmatrix} \begin{pmatrix} \tilde{F}_2(k) \\ \tilde{F}_3(k) \end{pmatrix} = E \begin{pmatrix} \tilde{F}_2(k) \\ \tilde{F}_3(k) \end{pmatrix}. \tag{3.30}$$

This would correspond to the valence and conduction band in a semiconductor. The above multiband equation has the solutions:

$$\begin{aligned} E(k) = &\frac{1}{2}\left(\frac{\hbar^2}{2m}(\gamma_{22}+\gamma_{33})k^2 + E_{2,0} + E_{3,0}\right) \\ &\pm \frac{1}{2}\sqrt{\left(\frac{\hbar^2}{2m}(\gamma_{22}-\gamma_{33})k^2 + E_{2,0} - E_{3,0}\right)^2 - 4\frac{\hbar^2}{m^2}p_{23}p_{32}k^2}. \end{aligned} \tag{3.31}$$

From the dispersion curves in Fig. 3 we see that the two band model is quite accurate within most of the first Brillouin zone, although this is by no means always the case, see, e.g., [15]. Note also that it is not generally possible to evaluate the infinite sum in Eq. (3.29), so we truncate it to a sufficient set of remote bands (elements of R). Usually we do not need to include that many remote bands as the denominator ensures that we can disregard remote bands sufficiently far away in energy from the energies of the set A.

3.2 Heterostructure example

In this section we study the example of a heterostructure consisting of N_b periods of one material, called the barrier material, and N_w periods of another material, called the well material, i.e., the potential is given by:

$$V(x) = (1-\theta_h(x))V_b(x) + \theta_h(x)V_w(x), \tag{3.32}$$

where $V_b(x)$ and $V_w(x)$ are bulk potentials with different V_0 and V values but the same period length a and

$$\theta_h(x) = \begin{cases} 1 & \text{for } -aN_b/2 < x < aN_b/2, \\ 0 & \text{else,} \end{cases} \tag{3.33}$$

for $x \in [-a(N_b+N_w)/2, a(N_b+N_w)/2]$, see Fig. 4 for an example. We impose periodic boundary conditions on the outside of our structure, i.e., we extend V to $\Omega = \mathbb{R}$ periodically and impose $F_n(x+NL) = F_n(x)$ for all $N = \mathbb{Z}$, where $L = a(N_b+N_w)$. Alternatively,

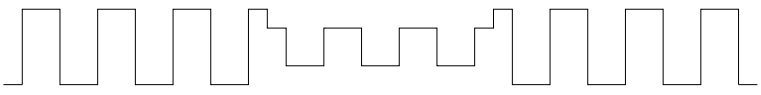

Figure 4: An example of the potential of a heterostructure.

we could use Dirichlet boundary conditions, however, we are mainly interested in bound states and they are unaffected (or weakly affected) by boundary conditions sufficiently far away from the well region. We use periodic boundary conditions in this case because they are natural for periodic structures as they would ensure translational invariance.

3.2.1 The k·p theory in practice and the appearance of spurious solutions

One of the major reasons for using k·p theory is to be able to use bulk values also in the case of a heterostructure. The bulk parameters are much easier to determine (either by ab initio calculations or experiments) than parameters appearing in the equations for a heterostructure derived above. Also, if bulk parameters can be used, we do not need to determine heterostructure parameters for each specific structure. For this reason, we would like to treat each material as a bulk material. This corresponds to working with different sets of periodic bases for each material and, as a result, the derivation of multiband equations needs to be modified, see [18]. Alternatively, bulk multiband models for the different materials can be used and connected via interface boundary conditions as discussed in Section 2. Which interface boundary conditions to use is still an active area of research and we do not enter this discussion here. Instead, we choose to use interface boundary conditions found using a symmetrization procedure as they serve to highlight why spurious solutions appear.

The multiband equation that we use is given by:

$$\sum_{n'}\left[-\frac{\hbar^2}{2m}\frac{\partial}{\partial x}\left(\gamma_{nn'}(x)\frac{\partial}{\partial x}\right)-i\frac{\hbar}{m}\left(\delta_{n<n'}p_{nn'}(x)\frac{\partial}{\partial x}+\delta_{n'<n}\frac{\partial}{\partial x}p_{nn'}(x)\right)+V_n(x)\delta_{nn'}\right]F_{n'}(x)$$
$$=EF_n(x), \tag{3.34}$$

where $\delta_{n<n'}=1$ for $n<n'$ and zero otherwise, $n,n'\in A$ and all parameters are stepwise constants with the bulk value in each material. Note that for our setup $p_{nn}=0$ as the periodic functions are either even or odd. There is no rigorous way of deriving this equation and the only arguments for using this specific form is that the set of equations are Hermitian (ensuring real eigen energies) and it reduces to the bulk equations in the case of a homogeneous material. There are other ways of deriving multiband equations, e.g. by using the quadratic response theory [16], however, this is outside the scope of this article. We only note that under these approaches the problem and the origin of spurious solutions remain the same as we address here. There are also other forms/choices which satisfy the same requirements (Hermitian system and reduction to the bulk system for homogeneous structures) and they are closely linked to the choice of interface boundary conditions. The interface boundary conditions can be found by integrating over a small volume around the interface and letting that volume go to zero. In our case the interface boundary conditions are continuity of

$$F_n(x) \text{ and } \sum_{n'}\left[\frac{\hbar^2}{2m}\left(\gamma_{nn'}(x)\frac{\partial}{\partial x}\right)+i\frac{\hbar}{m}\delta_{n'<n}p_{nn'}(x)\right]F_{n'}(x) \tag{3.35}$$

at the interface (continuity of $F_n(x)$ is necessary for the existence of the normal derivative at the interface). A different choice for the form of Eq. (3.34) would result in different interface boundary conditions.

Our two band model for a heterostructure is given by:

$$\begin{pmatrix} -\frac{\hbar^2}{2m}\frac{\partial}{\partial x}\gamma_{22}(x)\frac{\partial}{\partial x}+V_2(x) & -i\frac{\hbar}{m}p_{23}(x)\frac{\partial}{\partial x} \\ -i\frac{\hbar}{m}\frac{\partial}{\partial x}p_{32}(x) & -\frac{\hbar^2}{2m}\frac{\partial}{\partial x}\gamma_{33}(x)\frac{\partial}{\partial x}+V_3(x) \end{pmatrix}\begin{pmatrix} F_2(x) \\ F_3(x) \end{pmatrix}=E\begin{pmatrix} F_2(x) \\ F_3(x) \end{pmatrix}, \quad (3.36)$$

where V_2 and V_3 are given by the zone-center energies. In Fig. 5 we show a sketch of γ_{22} (the other parameters have a similar x dependence).

It turns out that in some cases the solutions to this kind of multiband equations are completely incorrect solutions in terms of the original problem (even in the cases where more accurate interface boundary conditions are used). In Fig. 6a) the energy spectrum is shown for a specific example. In between the solid lines is the band gap for the well material, i.e., the region in between bulk zone center energies $E_{2,0}$ and $E_{3,0}$. We do not expect to see solutions in the band gap, so this suggests that the energies highlighted by a circle are incorrect. In order to check that these solutions are wrong indeed, we have carried out calculations for the case where a finite but a large number of periodic functions have been used without treating the rest as remote bands, that is we have solved Eq. (3.10) including a large but finite U_n set. We have checked the accuracy of this approach by doubling the number of U_n states and comparing the eigen energies. It turns out that with a choice of the 10 lowest (in terms of energy) U_n, the error in the energies of interest is less than 0.1% (we refer further to these values, obtained with sufficient accuracy, as correct). The correct eigen energies are shown in Fig. 6b). From the two figures it is clear that the energies with a circle around are incorrect solutions. These solutions are known as spurious solutions as they have nothing to do with the original problem, although they are correct solutions to the multiband equation.

Our model is, in reality, over-specified. Indeed, the two band model (Eq. (3.36)) together with periodic boundary conditions and interface boundary conditions (Eq. (3.35)) result in 8 linear independent equations for the 8 unknown coefficients of the general solutions (4 general solutions in each material region). However, we also have the requirement that the Fourier expansion should be restricted to small k components. It is this last requirement which is not satisfied for the spurious solutions. In Fig. 7 we show the envelope function F_2 and its Fourier coefficients. We see that the major Fourier components are outside the first Brillouin zone. There are two separate issues here. First, from the exact envelope function theory we have the requirement that the Fourier expansion of the envelope function should be restricted to the first Brillouin zone to ensure uniqueness. This is not a major problem, however, as relaxing uniqueness requirements has been discussed in the literature, see [6]. Second, the assumption that $\hat{H}^1$ is small relies heavily on the assumption that only small k components of the envelope functions are non-zero. This can be seen from the bulk expression (Eq. (3.27)) that is used to derive the differential equations for each separate material (the first and second terms grow

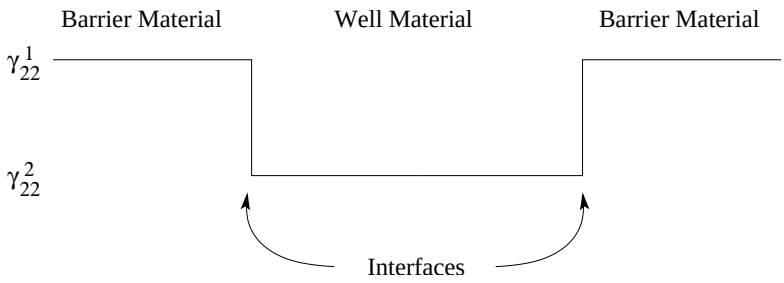

Figure 5: A schematic picture showing the spatial dependence of γ_{22}.

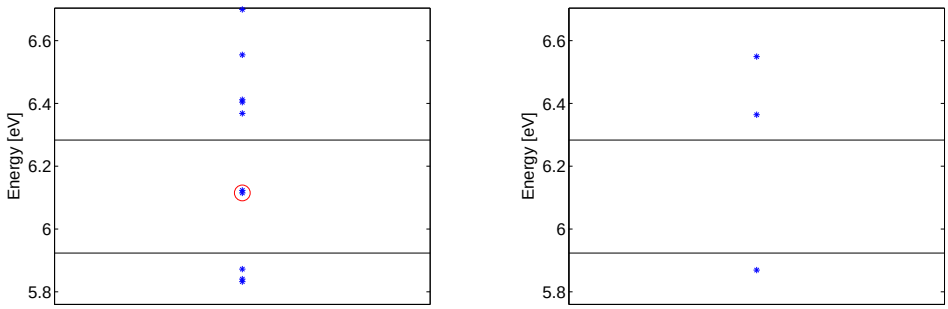

Figure 6: The bound states (the energies in the band gap of the barrier material) for a heterostructure consisting of 20 well and 20 barrier periods. The solid lines show the location of the bulk zone center energies $E_{2,0}$ and $E_{3,0}$ of the well material. The barrier potential is given by $V_{b0}=0$ eV, $V_b=5$ eV, the well potential is given by $V_{w0}=0$ eV, $V_w=3$ eV and $a=5$ Å. a) The energies calculated using the heuristic two band model. b) The correct energies.

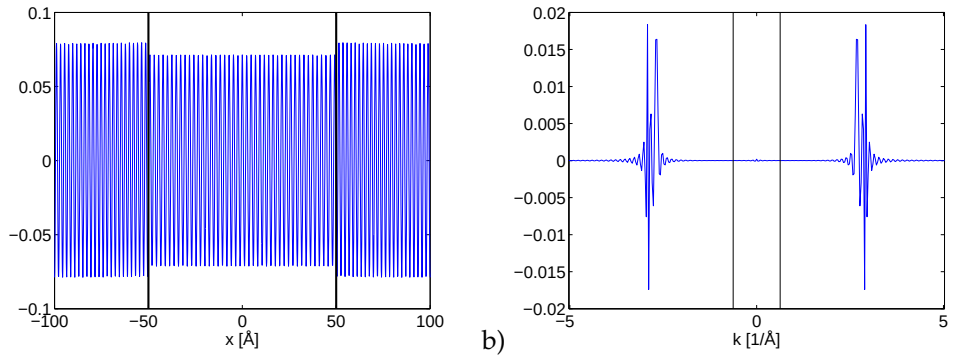

Figure 7: a) The real part of the envelope function F_2 (the imaginary part is zero). The solid vertical black lines show the location of the interfaces. b) The real part of the Fourier coefficients of the F_2 (the imaginary part is zero), the solid vertical lines show the boundary of the first Brillouin zone. The same parameters as in Fig. 6 have been used.

quadratically and linearly with k, respectively). So if we have non-zero components for large k values, the procedure used to derive multiband equations breaks down. The reason why the spurious solutions appear is that large k components are needed to satisfy the interface boundary conditions. So the problem with spurious solutions is that what would normally be considered a complete set of interface boundary conditions, i.e., $2N$ boundary conditions for a N band model, results in an over-specified problem, hence a reduced set of interface boundary conditions is needed. For approaches along these lines see, e.g., [20,77].

Table 1: The energies of the bound states. All energies are in eV. The same parameters as in Fig. 6 have been used.

Exact	Two Band	Two Band with Cut-Off
	5.7292	
	5.8325	
	5.8405	
5.8690	5.8723	5.8723
	6.1151	
	6.1229	
6.3643	6.3681	6.3682
	6.4042	
	6.4115	
6.5501	6.5546	6.5546
	6.6995	
	6.7062	

Another way of getting around this problem is to reformulate the set of coupled equations in k space and to restrict the problem to the first Brillouin zone (or in some cases to a smaller region in k space, see [104]). In order to implement this idea, we expand the solutions in plane waves and make a cut-off beyond a small neighborhood of $k=0$, see, e.g., [104]. In Table 1 we show the energy spectrum found using this approach together with both the correct energy spectrum and the energy spectrum found using the two band model. We see that energies found using the cut-off approach have an error of less than 0.1% compared to the correct energies. This shows that the present approach combined with plane wave cut-off removes the spurious solutions and gives quite accurate results. In general there are no fixed rules as to choosing the cut-off point. A good rule of thumb is to make the cut-off before the bulk dispersion curves enter the band gap. However, this does not ensure that the solutions are accurate as the assumptions behind k·p theory still fail for large k components even if there are no spurious solutions. In our case we made the cut-off at the edge of the first Brillouin zone. For more complicated multiband models, e.g., the eight-band model, the cut-off should be made much sooner. We will look at this issue further in Section 4.1. In Fig. 8a) we show the correct wave function together with the wave function found using the two band model with plane

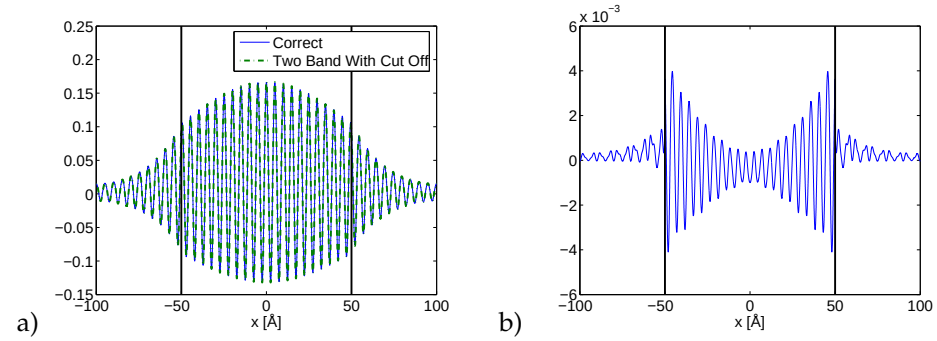

a) b)

Figure 8: a) The wave function found using the exact approach (20 bands included) together with the wave function found using the two band model with plane wave cut-off. b) The difference between the two wave functions. The same parameters as in Fig. 6 have been used.

wave cut-off. The wave function of the two band model is given by

$$\psi_{TwoBand}(x) = \sum_{n=2}^{3} F_n(x)\left[u_{n,0,b}(x)(1-\theta_h(x)) + \theta_h(x)u_{n,0,w}(x)\right], \tag{3.37}$$

where $u_{n,0,b}(x)$ are the zone-center solutions for the barrier and $u_{n,0,w}(x)$ are the zone-center solutions for the well. That is, we have taken into account that the periodic bases are different in the well and the barrier. The correct wave function is given by

$$\psi_{Correct}(x) = \sum_{n=1}^{N} F_n(x)u_{n,0,b}(x), \tag{3.38}$$

where N is the number of periodic solutions included in the calculations. From Fig. 8a) it is not easy to see any difference between the two solutions. Hence, in order to quantify the error introduced by using the two band model with cut-off we also show the difference between the two (Fig. 8b)). These figures show that the wave function too is well captured by the two band model with plane wave cut-off. We also note that the difference between the two solutions is largest close to the interfaces. We have made no attempt to model the interface more accurately, so this is not surprising. Using a more correct procedure to model the interface would result in increased accuracy of the two band wave function around the interfaces.

We point out that by using the cut-off approach we are actually solving a slightly different problem compared to the original two band differential equation (Eq. 3.36). This is most easily seen by noting that the original interface boundary conditions are not satisfied anymore as the envelope functions within the cut-off approach are smooth and the interface boundary conditions give rise to discontinuities in the first derivative of the envelope functions. The ordering of the material dependent parameters, i.e., the interface boundary conditions, is still an issue, however, as different orderings will result in different k space equations. For example, a term like

$$-\frac{\hbar^2}{2m}\frac{\partial}{\partial x}\gamma_{22}(x)\frac{\partial}{\partial x} \tag{3.39}$$

gives in k space rise to

$$\frac{\hbar^2}{2m}k\tilde{\gamma}_{22}(k-k')k', \tag{3.40}$$

and a term like

$$-\frac{\hbar^2}{2m}\gamma_{22}(x)\frac{\partial^2}{\partial x^2} \tag{3.41}$$

gives in k space rise to

$$\frac{\hbar^2}{2m}\tilde{\gamma}_{22}(k-k')k'k'. \tag{3.42}$$

A disadvantage of using plane wave expansions is that the resulting matrix eigenvalue problem is a problem where most of the elements of the matrix will be non-zero, as opposed to such approaches as finite element methods, which give rise to sparse problems and lead to the efficient analysis of low dimensional nanostructures [62, 99]. From a computational point of view, it is a concern because the full problem becomes more computationally demanding and hard to parallelize.

Another issue in working with plane waves with cut-off is that it is not obvious how to reduce the complexity of a problem using symmetries of the system. For example, if we have a three dimensional cylindrically symmetric problem, it is not obvious how to use this symmetry and at the same time to restrict the Fourier component to small k. This latter issue can be resolved and we do this in the next section.

4 Reduction of 3D models for nanostructures with cylindrical symmetry

In this section we consider three dimensional problems with cylindrical symmetry. The theory of Section 3 can easily be extended to three dimensions, see [5]. The focus of this section is on how to reduce the problem to a two dimensional problem and at the same time to ensure that the envelope functions are restricted to small k components. To simplify matters we choose to use the one band model for a cubic heterostructure:

$$\hat{H}\psi = [-\langle\nabla, A(\vec{r})\nabla\rangle + V(\vec{r})]\psi(\vec{r}) = E\psi(\vec{r}), \tag{4.1}$$

where $A(\vec{r}) = \frac{\hbar^2}{2m^*(\vec{r})}$, m^* is the effective mass, V is the effective potential (the conduction band edge), ∇ is the gradient. The effective mass is, in terms of the γ parameters of Section 3.1, given by $1/m^* = \gamma_{SS}/m$, where S denotes the periodic zone-center solution for the conduction band. The gradient of f is defined by:

$$\langle\vec{v}, \nabla f\rangle = D_{\vec{v}}f, \tag{4.2}$$

where $\langle\cdot,\cdot\rangle$ is the Euclidean inner product in $\mathbb{R}^3$. The problem is cylindrically symmetric as long as the effective mass m^*, the effective potential V and the domain of our system

Ω are cylindrically symmetric. For simplicity we assume that $\Omega=\mathbb{R}^3$. We are looking for solutions in the form:

$$\psi(\vec{r})=\int_{\Omega_k}\hat{\psi}(\vec{k})e^{i\langle\vec{k},\vec{r}\rangle}d^3k, \tag{4.3}$$

where Ω_k is a small neighborhood of $\vec{k}=0$ to be defined later (it needs to reflect the cylindrical symmetry). Using

$$\nabla e^{i\langle\vec{k},\vec{r}\rangle}=i\vec{k}e^{i\langle\vec{k},\vec{r}\rangle}, \tag{4.4}$$

we can reformulate the one band model in k space as follows:

$$\int_{\Omega_k}[\langle\vec{k}',\hat{A}(\vec{k}',\vec{k})\vec{k}\rangle+\hat{V}(\vec{k}',\vec{k})]\hat{\psi}(\vec{k})d^3k=E\hat{\psi}(\vec{k}'), \tag{4.5}$$

where

$$\hat{A}(\vec{k}',\vec{k})=\frac{1}{(2\pi)^3}\int_{\Omega}A(\vec{r})e^{i\langle\vec{k}-\vec{k}',\vec{r}\rangle}d^3r \text{ and } \hat{V}(\vec{k}',\vec{k})=\frac{1}{(2\pi)^3}\int_{\Omega}V(\vec{r})e^{i\langle\vec{k}-\vec{k}',\vec{r}\rangle}d^3r. \tag{4.6}$$

Due to the cylindrical symmetry we know that

$$[\hat{H},\hat{S}_\theta]=0, \tag{4.7}$$

where $[\cdot,\cdot]$ is the commutator, $\hat{S}_\theta f(\vec{r})=f(S_\theta\vec{r})$ for any function f and S_θ is the operator that rotates $\mathbb{R}^3$ by the angle θ around the symmetry axis. Choosing the Cartesian coordinates ($\vec{r}=(x,y,z)$) where the third axis points along the symmetry axis, we have:

$$S_\theta=\begin{pmatrix}\cos(\theta) & -\sin(\theta) & 0\\ \sin(\theta) & \cos(\theta) & 0\\ 0 & 0 & 1\end{pmatrix}. \tag{4.8}$$

Because of the commutation relation (4.7) we can find wave functions ψ which are simultaneous eigen solutions of $\hat{S}_\theta$, i.e., we can find solutions ψ_l so that:

$$\hat{S}_\theta\psi_l=e^{il\theta}\psi_l, \tag{4.9}$$

where l is an integer. This can be verified by differentiating the eigenvalue problem $\hat{S}_\theta\psi=\lambda_\theta\psi$ with respect to θ, evaluating it at $\theta=0$, and using the periodicity condition $S_\theta=S_{\theta+2\pi}$. Using the Fourier expansion we have:

$$\begin{aligned}e^{il\theta}\psi_l(\vec{r})&=\hat{S}_\theta\psi_l(\vec{r})\\ &=\psi_l(S_\theta\vec{r})\\ &=\int_{\Omega_k}\hat{\psi}_l(\vec{k})e^{i\langle\vec{k},S_\theta\vec{r}\rangle}d^3k\\ &=\int_{\Omega_k}\hat{\psi}_l(\vec{k})e^{i\langle S_{-\theta}\vec{k},\vec{r}\rangle}d^3k\\ &=\int_{\Omega_k}\hat{\psi}_l(S_\theta\vec{k})e^{i\langle\vec{k},\vec{r}\rangle}d^3k.\end{aligned} \tag{4.10}$$

From this it is easily seen that:

$$e^{il\theta}\hat{\psi}_l(\vec{k}) = \hat{\psi}_l(S_\theta \vec{k}). \tag{4.11}$$

This equation has the solution:

$$\hat{\psi}_l(\vec{k}) = e^{il\theta_k}\tilde{\psi}(k,k_z), \tag{4.12}$$

where

$$k_x = k\cos(\theta_k) \text{ and } k_y = k\sin(\theta_k). \tag{4.13}$$

Using cylindrical coordinates

$$x = r\cos(\theta_r) \text{ and } y = r\sin(\theta_r) \tag{4.14}$$

and using the fact that A is a function of r and z only we find:

$$\begin{aligned}
\hat{A}(\vec{k}',\vec{k}) &= \frac{1}{(2\pi)^3}\int A(r,z)e^{i(kr\cos(\theta_k-\theta_r)-k'r\cos(\theta_{k'}-\theta_r)+(k_z-k_z')z)}rdrd\theta_r dz \\
&= \frac{1}{(2\pi)^3}\int A(r,z)\sum_{n,n'}(i)^{n+n'}J_n(kr)J_{n'}(-k'r)e^{in(\theta_k-\theta_r)}e^{-in'(\theta_{k'}-\theta_r)}e^{i(k_z-k_z')z}rdrd\theta_r dz \\
&= \frac{1}{(2\pi)^3}\int A(r,z)\sum_{n,n'}(i)^{n+n'}(-1)^{n'}J_n(kr)J_{n'}(k'r)e^{i(n\theta_k-n'\theta_{k'})}e^{i(n'-n)\theta_r}e^{i(k_z-k_z')z}rdrd\theta_r dz \\
&= \frac{1}{(2\pi)^2}\int A(r,z)\sum_{n}J_n(kr)J_n(k'r)e^{in(\theta_k-\theta_{k'})}e^{i(k_z-k_z')z}rdrdz,
\end{aligned} \tag{4.15}$$

where we have used that:

$$e^{ix\cos(\phi)} = \sum_n i^n J_n(x)e^{i\phi n}, \tag{4.16}$$

and the domain of integration is

$$0 \le r < r_{\max}(z), \quad z_{\min} < z < z_{\max}, \quad 0 \le \theta < 2\pi.$$

Here $z_{\min}$, $z_{\max}$ and $r_{\max}(z)$ are determined by Ω. In the case where $\Omega = \mathbb{R}^3$ we have $z_{\min} = -\infty$, $z_{\max} = \infty$ and $r_{\max}(z) = \infty$. The same arguments apply to $\hat{V}$:

$$\hat{V}(\vec{k}',\vec{k}) = \frac{1}{(2\pi)^2}\int V(r,z)\sum_n J_n(kr)J_n(k'r)e^{in(\theta_k-\theta_{k'})}e^{i(k_z-k_z')z}rdrdz. \tag{4.17}$$

We are now in a position to integrate out all angle dependent terms in the one band model, Eq. (4.5). Assuming that the region in k space Ω_k is given by $k_{z,\min} < k_z < k_{z,\max}$,

$0\leq k<k_{\max}$ and $0\leq\theta_k<2\pi$ we get:

$$\begin{aligned}
&2\pi E\tilde{\psi}(k',k'_z)\\
&=\int\left[\hat{A}(\vec{k}',\vec{k})(kk'\cos(\theta'_k-\theta_k)+k'_zk_z)\right]e^{il\theta_k}\tilde{\psi}(k,k_z)e^{-il\theta_{k'}}kdkd\theta_kdk_zd\theta_{k'}\\
&\quad+\int\hat{V}(\vec{k}',\vec{k})e^{il\theta_k}\tilde{\psi}(k,k_z)e^{-il\theta_{k'}}kdkd\theta_kdk_zd\theta_{k'}\\
&=\frac{1}{(2\pi)^2}\int A(r,z)\sum_n J_n(kr)J_n(k'r)e^{in(\theta_k-\theta_{k'})}e^{i(k_z-k'_z)z}r\\
&\qquad\times\left[kk'\cos(\theta_{k'}-\theta_k)+k'_zk_z\right]e^{il\theta_k}\tilde{\psi}(k,k_z)e^{-il\theta_{k'}}kdrdzdkd\theta_kdk_zd\theta_{k'}\\
&\quad+\frac{1}{(2\pi)^2}\int V(r,z)\sum_n J_n(kr)J_n(k'r)e^{in(\theta_k-\theta_{k'})}e^{i(k_z-k'_z)z}r\\
&\qquad\times e^{il\theta_k}\tilde{\psi}(k,k_z)e^{-il\theta_{k'}}kdrdzdkd\theta_kdk_zd\theta_{k'}\\
&=\frac{1}{2}\int A(r,z)(kk'\left[J_{-l-1}(kr)J_{-l-1}(k'r)+J_{-l+1}(kr)J_{-l+1}(k'r))+k'_zk_zJ_{-l}(kr)J_{-l}(k'r)\right]\\
&\qquad\times e^{i(k_z-k'_z)z}\tilde{\psi}(k,k_z)krdrdzdkdk_z\\
&\quad+\int V(r,z)J_{-l}(kr)J_{-l}(k'r)e^{i(k_z-k'_z)z}\tilde{\psi}(k,k_z)krdrdzdkdk_z.
\end{aligned}\tag{4.18}$$

All in all, we have:

$$\begin{aligned}
E\tilde{\psi}(k',k'_z)=&\int_{k_{z,\min}}^{k_{z,\max}}\int_0^{k_{\max}}\frac{\tilde{A}_{l+1}(k',k'_z,k,k_z)+\tilde{A}_{l-1}(k',k'_z,k,k_z)}{2}k'k\tilde{\psi}(k,k_z)dkdk_z\\
&+\int_{k_{z,\min}}^{k_{z,\max}}\int_0^{k_{\max}}\tilde{A}_l(k',k'_z,k,k_z)k'_zk_z\tilde{\psi}(k,k_z)dkdk_z\\
&+\int_{k_{z,\min}}^{k_{z,\max}}\int_0^{k_{\max}}\tilde{V}_l(k',k'_z,k,k_z)\tilde{\psi}(k,k_z)dkdk_z,
\end{aligned}\tag{4.19}$$

where

$$\tilde{A}_l(k',k'_z,k,k_z)=\frac{k}{2\pi}\int_{z_{\min}}^{z_{\max}}\int_0^{r_{\max}(z)}A(r,z)J_l(kr)J_l(k'r)e^{i(k_z-k'_z)z}rdrdz,\tag{4.20}$$

$$\tilde{V}_l(k',k'_z,k,k_z)=\frac{k}{2\pi}\int_{z_{\min}}^{z_{\max}}\int_0^{r_{\max}(z)}V(r,z)J_l(kr)J_l(k'r)e^{i(k_z-k'_z)z}rdrdz,\tag{4.21}$$

and we have used $J_{-l}(x)=(-1)^lJ_l(x)$.

We have now reduced the problem to a two dimensional problem while ensuring that the Cartesian plane wave expansion is restricted to small $\mathbf{k}$ components. It is not surprising that the radial part should be expanded in Bessel functions as these functions are the radial solutions to the Laplace eigenvalue equation in cylindrical coordinates. It is, however, not initially obvious that restricting to small k components of the Bessel

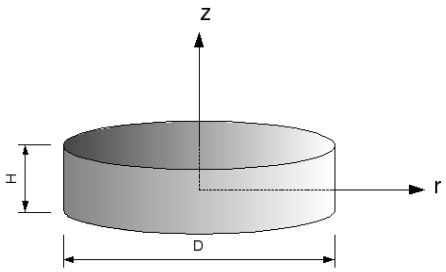

Figure 9: The cylindrical InAs quantum dot under consideration. The matrix material is GaAs.

functions (and k_z components) is equivalent to the restriction to small $\mathbf{k}$ components. But this is indeed the case as can be seen from Eq. (4.13).

This approach can easily be extended to multiband models as long as they are cylindrically symmetric. In the next section we will present results for a cylindrical InAs quantum dot imbedded in a GaAs matrix.

4.1 The eight-band model results

Here we consider an InAs cylindrical quantum dot surrounded by GaAs (see Fig. 9). For a discussion on the cylindrically symmetric eight-band model for zincblende nanostructures we refer the reader to [74]. In what follows, the material parameters are taken from [88] and they are reproduced here for convenience in Table 2. In Fig. 10b) we show the energy spectrum as a function of the k space cut-off for a quantum dot with height $H = 10$ nm and diameter $D = 10$ nm. In this figure we see that the first couple of conduction and valence band states are well captured with a cut-off 25% out in the Brillouin zone. If we compare this to what happens for a quantum dot with a height and diameter of 5 nm (shown in Fig. 10a)), we see that we need to use a cut-off 60% out in the Brillouin zone to get convergence of the conduction band states. However, spurious solutions start to appear in the valence band before this. That is, we cannot capture both conduction and valence band states for such small dots using the cut-off approach. If we instead used the approach proposed in [13] we do not need to use a cut-off and we could get the states to converge. However, this does not ensure that the solutions are meaningful as the states have Fourier components far away from the zone center and we know that the accuracy of k·p methods using a zone center expansion basis decreases as we move away from the zone center.

Table 2: k·p parameters used. m_e is the free electron mass.

	$m_c\ [m_e]$	γ_1	γ_2	γ_3	$E_g\ [eV]$	$\Delta_{so}\ [eV]$	$E_p\ [eV]$	VBO
InAs	0.026	20.0	8.5	8.5	0.417	0.39	21.5	-0.59
GaAs	0.067	6.98	2.06	2.06	1.519	0.341	28.8	-0.8

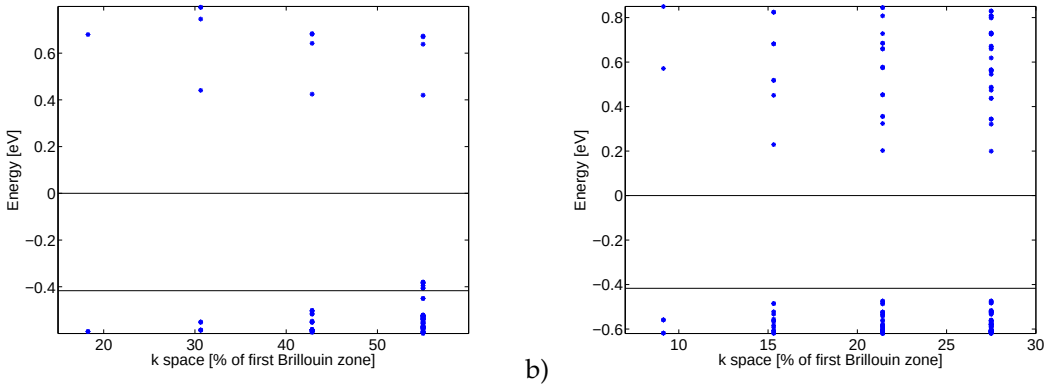

Figure 10: Energy spectra as a function of k space cut-off for a) $H=D=5$ nm and b) $H=D=10$ nm. The black lines are the valence and conduction band edges of InAs.

4.2 Gap states and spurious solutions

Finally, we note that the above discussion is related to the issue of finding gap states in quantum-confined structures using the $\mathbf{k}\cdot\mathbf{p}$ method, and we will now briefly address this issue. Recall that in the past multiband $\mathbf{k}\cdot\mathbf{p}$ Hamiltonian calculations have been carried out to find the S and P states representing the lower conduction band and the upper valence band (e.g., [80, 89]). The Hamiltonian problem in this case has been solved as a coupled system of PDEs (see [80, 89]), and there is no a priori guarantee that the resulting solutions contain only wavevector components in the first Brillouin zone. In actual fact, the non-physical gap states produced by solving such coupled system of PDEs (as in [80,89]) contain out-of-first Brillouin-zone wavevector components and hence must be rejected as non-physical solutions [5]. A secure way to circumvent this problem in $\mathbf{k}\cdot\mathbf{p}$ calculations is to use a plane-wave expansion set containing first Brillouin-zone components only. This is exactly what has been proposed in the present work.

5 Conclusions and future directions

In this paper we focused on a long standing problem in the application of the multiband effective mass theory to low dimensional nanostructures that manifests itself in the appearance of non-physical (spurious) solutions. Due to its fundamental significance and a wide range of applications in science and engineering, there have been a substantial number of attempts to resolve this problem. We reviewed some of such approaches together with available techniques for formulating interface boundary conditions for the associated model for the envelope functions and discussed this issue in a broader context of other computationally efficient methods for bandstructure calculations. Next, based our discussion of the generalized envelope function theory, we derived multiband equations for the one dimensional case. We demonstrated that a failure to restrict the Fourier

expansion of the envelope functions to small k components, which is in the heart of the multiband model derivation, may lead to spurious solutions with no physical meaning. On an example of a heterostructure, we provided details of a procedure of how such non-physical solutions can be removed and evaluated the accuracy of the results obtained. We exemplified this approach by a reduction of a three dimensional cylindrically symmetric problem to a two dimensional problem within the plane wave cut-off approach. The resulting model provides a computationally efficient framework for the analysis of cylindrical symmetric systems and we demonstrated the efficiency of our developed multiband model in applications to cylindrically symmetric quantum dots.

Finally, we note that an appropriate choice of the basis for our multiband model may bring further computational advantages leading to the effect of the Gibbs phenomenon being minimized while moving from the **k**-space to the real physical space. The resulting systems of linear equations will be sparse, as we pointed out in Section 2, reducing further the computational cost and providing additional advantages of this methodology as compared to ab initio and atomistic techniques. This issue deserves further discussion in a separate publication.

Acknowledgments

This work was supported by the Hans Christian Andersen Academy, the NSERC and CRC Programs, and the Quest Framework Program. R.M. acknowledges the hospitality of the Isaac Newton Institute at the University of Cambridge and thank the organizers of the HOP Programme for the productive environment created during the course of the programme.

Appendix

As we pointed out in the introductory part, the determination of the energy operator spectrum is formulated throughout one Brillouin zone and the first Brillouin zone is usually taken for this purpose. Any periodic lattice is completely specified by its principle lattice vectors $\mathbf{a}_1$,$\mathbf{a}_2$ and $\mathbf{a}_3$ defined such that any translation vector $\mathbf{R}$ (a vector connecting two lattice points) can be written as:

$$\mathbf{R}=m_1\mathbf{a}_1+m_2\mathbf{a}_2+m_3\mathbf{a}_3, \tag{A.1}$$

for some $m_1,m_2,m_3\in\mathbb{Z}$. Based on the principle lattice vectors, the reciprocal lattice can be defined as those vectors $\mathbf{b}$ that satisfy:

$$\exp(i\mathbf{b}\mathbf{R})=1. \tag{A.2}$$

It can be shown that any reciprocal lattice vector is given by:

$$\mathbf{b}=n_1\mathbf{b}_1+n_2\mathbf{b}_2+n_3\mathbf{b}_3, \tag{A.3}$$

for some $n_1, n_2, n_3 \in \mathbb{Z}$, where

$$\mathbf{b}_1 = 2\pi/\Omega_0[\mathbf{a}_2 \times \mathbf{a}_3], \quad \mathbf{b}_2 = 2\pi/\Omega_0[\mathbf{a}_3 \times \mathbf{a}_1],$$
$$\mathbf{b}_3 = 2\pi/\Omega_0[\mathbf{a}_1 \times \mathbf{a}_2], \quad \Omega_0 = \mathbf{a}_1[\mathbf{a}_2 \times \mathbf{a}_3].$$

Of course, there are many reasons for the construction of the reciprocal lattice, but the one we focus on here is its relation to irreducible representations of the translational group related to the translation vectors **R** (that is the translational symmetry of the system). It can be shown that any irreducible representation of the translational group is completely determined by

$$\lambda_1 = \exp(-i\mathbf{k}\mathbf{a}_1), \quad \lambda_2 = \exp(-i\mathbf{k}\mathbf{a}_2), \quad \lambda_3 = \exp(-i\mathbf{k}\mathbf{a}_3),$$

where vector **k** is determined up to an arbitrary reciprocal lattice vector, see [3]. The ambiguity in **k** is completely removed by restricting our attention to the first Brillouin zone (the Wigner-Seitz cell of the reciprocal lattice).

References

[1] P.V. Avramov et al., Density-functional theory study of the electronic structure of thin Si/SiO2 quantum nanodots and nanowires, Phys. Rev. B, 75 (20), 205427, 2007.
[2] G. Bastard Wave mechanics applied to semiconductor heterostructures. New York: Halsted Press (a division of John Wiley & Sons), 1988.
[3] G.L. Bir, G.E. Pikus Symmetry and strain-induced effects in semiconductors. New York: Wiley, 1974.
[4] M. G. Burt. An exact formulation of the envelope function method for the determination of electronic states in semiconductor microstructure. Semicond. Sci. Technol., 3, 739, 1988.
[5] M.G. Burt, The justification for applying the effective-mass approximation to microstructures, J. Phys. Cond. Matt. 4, 6651, 1992.
[6] M. G. Burt. Resolution of the out-of-zone solution problem in envelope-function theory. Superlatt. Microstruct., 23, 531, 1998.
[7] M.G. Burt, Fundamentals of envelope function theory for electronic states and photonic modes in nanostructures, J. Phys.: Condens. Matter, 11, R53-R83, 1999.
[8] B. Chen, M. Lazzouni, and L. R. Ram-Mohan. Diagonal representation for the transfer-matrix method for obtaining electronic energy levels in layered semiconductor heterostructures. Phys. Rev. B, 45 (3), 1204-1212, 1992.
[9] J. P. Cuypers and W. van Haeringen. Connection rules for envelope functions at semiconductor-heterostructure interfaces. Phys. Rev. B, 47 (16), 10310-10318, 1993.
[10] J. H. Davies The physics of low-dimensional semiconductors. Cambridge: Cambridge University Press, 1998.
[11] E. Ertekin, P.A. Greaney, and D.C. Chrzan, Equilibrium limits of coherency in strained nanowire heterostructures, J. of Applied Physics, 97, 114325, 2005.
[12] B. A. Foreman, Effective-mass Hamiltonian and boundary conditions for the valence bands of semiconductor microstructures, Phys. Rev. B, 48 (7), 4964–4967, 1993.
[13] B. A. Foreman. Elimination of spurious solutions from eight-band k·p theory. Phys. Rev. B, 56, R12748, 1997.

[14] B. A. Foreman. Connection rules versus differential equations for envelope functions in abrupt heterostructures. Phys. Rev. Lett., 80 (17), 3823-3826, 1998.
[15] B. A. Foreman. Choosing a basis that eliminates spurious solutions in k·p theory. Phys. Rev. B, 75 (23), 235331, 2007.
[16] B. A. Foreman. Valence-band mixing in first-principles envelope-function theory. Phys. Rev. B, 76 (4), 043327, 2007.
[17] B. A. Foreman. First-principles envelope-function theory for lattice-matched semiconductor heterostructures. Phys. Rev. B (Condensed Matter and Materials Physics), 72 (16), 165345, 2005.
[18] B. A. Foreman. Envelope-function formalism for electrons in abrupt heterostructures with material-dependent basis functions. Phys. Rev. B, 54, 1909, 1996.
[19] C. Galeriu et al., Modeling a nanowire superlattice using the finite difference method in cylindrical polar coordinates, Computer Physics Communications, 157 (2), 147-159, 2004.
[20] M. J. Godfrey and A. M. Malik. Boundary conditions and spurious solutions in envelope-function theory. Phys. Rev, B, 53, 16504, 1996.
[21] J.X. Han et al., Real space method for the electronic structure of one-dimensional periodic systems, Journal of Chemical Physics, 129 (14), 144109, 2008.
[22] M. Heiskanen et al., Multigrid method for electronic structure calculations, Phys. Rev. B, 63, 245106, 2001.
[23] P. Huang, E.A. Carter, Advances in correlated electronic structure methods for solids, surfaces, and nanostructures, Annual Review of Physical Chemistry, 59, 261-290, 2008.
[24] A. Iserles, S. P. Norsett, and S. Olver, Highly oscillatory quadrature: The story so far, Proceedings of ENuMath, Santiago de Compostela, A. Bermudez de Castro et al., (eds.), Springer-Verlag, Berlin, 97-118, 2006.
[25] R. Khare et al., Multiscale coupling schemes spanning the quantum mechanical, atomistic forcefield, and continuum regimes, Computer Methods in Applied Mechanics and Engineering, 197 (41-42), 3190-3202, 2008.
[26] K.I. Kolokolov, J. Li, and C.Z. Ning, $k\cdot p$ Hamiltonian without spurious-state solutions, Phys. Rev. B, 68, 161308(R), 2003.
[27] B. Lassen B, L. C. Lew Yan Voon, M Willatzen, R. V. N. Melnik. Exact envelope-function theory versus symmetrized Hamiltonian for quantum wires: a comparison. Solid State Communications, 132 (3-4), 141-149, 2004.
[28] B. Lassen, M. Willatzen, R. Melnik and L. C. Lew Yan Voon, A General Treatment of Deformation Effects in Hamiltonians for Inhomogeneous Crystalline Materials, Journal of Mathematical Physics, Vol. 46, 112102, 2005.
[29] B. Lassen, M. Willatzen, R. Melnik, Inclusion of nonlinear strain effects in the Hamiltonian for nanoscale semiconductor structures, Journal of Computational and Theoretical Nanoscience, 3 (4), 588-597, 2006.
[30] B. Lassen, M. Willatzen, R. Melnik, and L. C. Lew Yan Voon, Electronic properties of free-standing InP and InAs nanowires, J. Mater. Res., 21 (11), 2927-2935, 2006.
[31] B. Lassen, M. Willatzen, R. Melnik and L. C. Lew Yan Voon, Spurious solutions and boundary conditions in $k\cdot p$ theory, Proc. 28th Int. Conf. Phys. Semi., AIP Conf. Proc., 893, 993-994, 2007.
[32] S. Lee, F. Oyafuso, P. von Allmen, and G. Klimeck, Boundary conditions for the electronic structure of finite-extent, embedded semiconductor nanostructures, Phys. Rev. B, 69 (4), 045316, 2004.
[33] L. Lew Yan Voon, R. Melnik, B. Lassen, M. Willatzen, Influence of aspect ratio on the lowest

states of quantum rods, Nano Letters, 4 (2), 289-292, 2004.
[34] L. Lew Yan Voon, R. Melnik, B. Lassen, M. Willatzen, Prediction of barrier localization in modulated nanowires, Journal of Applied Physics, 96 (8), 4660-4662, 2004.
[35] L. Lew Yan Voon, C. Galiriu, B. Lassen et al., Electronic structure of wurtzite quantum dots with cylindrical symmetry, Applied Physics Letters, 87 (4), 041906, 2005.
[36] L. C. Lew Yan Voon and M. Willatzen, The $\mathbf{k}\cdot\mathbf{p}$ Method - Electronic Bandstructure of Semiconductors, Springer Verlag Series on Solid State Physics, to appear in 2009.
[37] K. Lüdge, M. J. P. Bormann, E. Malic, P. Hövel, M. Kuntz, D. Bimberg, A. Knorr, and E. Schöll, Turn-on dynamics and modulation response in semiconductor quantum dot lasers, Phys. Rev. B, 78, 035316, 2008.
[38] M. Luisier, A. Schenk, Atomistic simulation of nanowire transistors, Journal of Computational and Theoretical Nanoscience, 5 (6), 1031-1045, 2008.
[39] J.M. Luttinger and W. Kohn, Motion of electrons and holes in perturbed periodic fields, Physical Review, 97 (4), 869–883, 1955.
[40] D.R. Mahapatra, R.V.N. Melnik, Three-dimensional mathematical models of phase transformation kinetics in shape memory alloys, Dynamics of Continuous Discrete and Impulsive Systems - Series B - Applications & Algorithms, Vol. 2, Sp. Iss. SI, 557-562, 2005.
[41] D.R. Mahapatra, R.V.N. Melnik, Finite element modelling and simulation of phase transformations in shape memory alloy thin films, International Journal for Multiscale Computational Engineering, 5 (1), 65-71, 2007.
[42] D.R. Mahapatra, R.V.N. Melnik, Finite element approach to modelling evolution of 3D shape memory materials, Mathematics and Computers in Simulation, 76 (1-3), 141-148, 2007.
[43] D. R. Mahapatra et al., Field emission from strained carbon nanotubes on cathode substrate, Applied Surface Science, 255 (5), 1959-1966, 2008.
[44] N. Malkova, C.Z. Ning, Band structure and optical properties of wurtzite semiconductor nanotubes, Phys. Rev. B, 75 (15), 155407, 2007.
[45] K.N. Melnik and R.V.N. Melnik, Optimal-by-order quadrature formulae for fast oscillatory functions with inaccurately given a priori information, Journal of Computational and Applied Mathematics, 110 (1), 45-72, 1999.
[46] K.N. Melnik and R.V.N. Melnik, Optimal cubature formulae and recovery of fast-oscillating functions from an interpolational class, BIT Numerical Mathematics, 41 (4), 748-775, 2001.
[47] K.N. Melnik and R.V.N. Melnik, Optimal-by-accuracy and optimal-by-order cubature formulae in interpolational classes, Journal of Computational and Applied Mathematics, 147 (1), 233-262, 2002.
[48] R.V.N. Melnik, Topological analysis of eigenvalues in engineering computations, Engineering Computations, 17 (4), 386-416, 2000.
[49] R.V.N. Melnik and H. He, Relaxation-time approximations of quasi-hydrodynamic type in semiconductor device modelling, Modelling and Simulation in Materials Science and Engineering, 8 (2), 133-149, 2000.
[50] R.V.N. Melnik and H. He, Quasi-hydrodynamic modelling and computer simulation of coupled thermo-electrical processes in semiconductors, Mathematics and Computers in Simulation, 52 (3-4), 273-287, 2000.
[51] R.V.N. Melnik and H. He, Modelling nonlocal processes in semiconductor devices with exponential difference schemes, Journal of Engineering Mathematics, 38 (3), 233-263, 2000.
[52] R.V.N. Melnik, Generalised solutions, discrete models and energy estimates for a 2D problem of coupled field theory, Applied Mathematics and Computation, 107 (1), 27-55, 2000.
[53] R.V.N. Melnik, Computational analysis of coupled physical fields in piezothermoelastic me-

dia, Computer Physics Communications, 142 (1-3), 231-237, 2001.
[54] R.V.N. Melnik, A.J. Roberts, Thermomechanical behaviour of thermoelectric SMA actuators, Journal de Physique IV, 11 (PR8), 515-520, 2001.
[55] R.V.N. Melnik, A.J. Roberts, Computational models for materials with shape memory: Towards a systematic description of coupled phenomena, Computational Science - ICCS 2002, PT II, Book Series: Lecture Notes in Computer Science, Vol. 2330, 490-499, 2002.
[56] R.V.N. Melnik, Modelling coupled dynamics: Piezoelectric elements under changing temperature conditions, International Communications in Heat and Mass Transfer, 30 (1), 83-92, 2003.
[57] R.V.N. Melnik, K.N. Zotsenko, Mixed electroelastic waves and CFL stability conditions in computational piezoelectricity, Applied Numerical Mathematics, 48 (1), 41-62, 2004.
[58] R. Melnik and R. Mahapatra, Coupled effects in quantum dot nanostructures with nonlinear strain and bridging modelling scales, Computers & Structures, 85 (11-14), 698-711, 2007.
[59] R.V.N. Melnik, K.N. Zotsenko, Computations of coupled electronic states in quantum dot/wetting layer cylindrical structures, Computational Science - ICCS 2003, Pt III, Proceedings, Lecture Notes in Computer Science, Vol. 2659, 343-349, 2003.
[60] R. V. N. Melnik, J. Rimshans, Numerical analysis of fast charge transport in optically sensitive semiconductors, Dynamics of Continuous Discrete and Impulsive Systems - Series B - Applications & Algorithms, Supplement: Suppl. S, 102-107, 2003.
[61] R. V. N. Melnik, M. Willatzen Bandstructures of conical quantum dots with wetting layers. Nanotechnology, 15 (1), 1–8, 2004.
[62] R.V.N. Melnik, K.N. Zotsenko, Finite element analysis of coupled electronic states in quantum dot nanostructures, Modelling and Simulation in Materials Science and Engineering, 12 (3), 465-477, 2004.
[63] R.V.N. Melnik, A. Povitsky, Wave phenomena in physics and engineering: new models, algorithms, and applications, Mathematics and Computers in Simulation, 65 (4-5), 299-302, 2004.
[64] R.V.N. Melnik, A. Roberts, Computational models for multi-scale coupled dynamic problems, Future Generation Computer Systems, 20 (3), 453-464, 2004.
[65] R.V.N. Melnik, A. Povitsky, A special issue on modelling coupled and transport phenomena in nanotechnology, Journal of Computational and Theoretical Nanoscience, 3 (4), pp. i-ii, 2006.
[66] R. Melnik, A. Povitsky, D. Srivastava, Mathematical and Computational Models for Transport and Coupled Processes in Micro- and Nanotechnology, Journal of Nanoscience and Nanotechnology, 8 (7), 3626-3627, 2008.
[67] R. Melnik, Multiple Scales and Coupled Effects in Modelling Low Dimensional Semiconductor Nanostructures: Between Atomistic and Continuum Worlds, Encyclopedia of Complexity and Systems Science, Springer, to appear, 2009.
[68] A. T. Meney, Besire Gonul, and E. P. O'Reilly. Evaluation of various approximations used in the envelope-function method. Phys. Rev. B, 50, 10893, 1994.
[69] M.O. Nestoklon, E.L. Ivchenko, J.M. Jancu, P. Voisin, Electric field effect on electron spin splitting in SiGe/Si quantum wells Phys. Rev. B, 77, 155328, 2008.
[70] T. Ono, K. Hirose, Real-space electronic-structure calculations with a time-saving double-grid technique, Phys. Rev. B, 72 (8), 085115, 2005.
[71] T. Ono, K. Hirose, Real-space density-functional calculations for transport properties of nanostructures, Journal of Computational and Theoretical Nanoscience, 4 (5), 840-859, 2007.
[72] M.L. Parks, P.B. Bochev, R.B. Lehoucq, Connecting atomistic-to-continuum coupling and

domain decomposition, Multiscale Modeling & Simulation, 7 (1), 362-380, 2008.
[73] D.J. Paul, 8-band $k \times p$ modeling of the quantum confined Stark effect in Ge quantum wells on Si substrates, Phys. Rev. B, 77, 155323, 2008.
[74] E.P. Pokatilov, V.A. Fonoberov, V.M. Fomin and J.T. Devrees Development of an eight-band theory for quantum dot heterostructures, Prys. Rev. B, 64, 245328-1, 2001.
[75] N. Radulovic et al., Resonant tunneling heterostructure devices - Dependencies on thickness and number of quantum wells, Computational Science and its Applications - - ICCSA 2004, PT 3 Book Series: Lecture Notes in Computer Science, Vol. 3045, 817-826, 2004.
[76] N. Radulovic et al., Influence of the metal contact size on the electron dynamics and transport inside the semiconductor heterostructure nanowire, Journal of Computational and Theoretical Nanoscience, 3 (4), 551-559, 2006.
[77] A. V. Rodina, A. Yu Alekseev, Al. L. Elfros, M. Rosen, and B. K. Meyer. General boundary conditions for the envelope fnuction in the multiband k·p model. Phys. Rev. B, 65, 125302–1, 2002.
[78] A.V. Rodina and A.Y. Alekseev, Least-action principle for envelope functions in abrupt heterostructures, Phys. Rev. B, 73, 115312, 2006.
[79] A. Schliwa, M. Winkelnkemper, and D. Bimberg, Impact of size, shape, and composition on piezoelectric effects and electronic properties of In(Ga)As/GaAs quantum dots, Phys. Rev. B, 76, 205324, 2007.
[80] P.C. Sercel, A. L. Efros, and M. Rosen, Intrinsic gap states in semiconductor nanocrystals, Phys. Rev. Lett., 83, 2394, 1999.
[81] J. Singh Physics of semiconductors and their heterostructures. New York: McGraw-Hill, 1993.
[82] N. Sinha et al., Carbon nanotube thin film field emitting diode: Understanding the system response based on multiphysics modeling, Journal of Computational and Theoretical Nanoscience, 4 (3), 535-549, 2007.
[83] N. Sinha et al., Electromechanical interactions in a carbon nanotube based thin film field emitting diode, Nanotechnology, 19 (2), 025701, 2008.
[84] J.C. Slater, Electrons in perturbed periodic lattices, Physical Review, 76 (11), 1592–1601, 1949.
[85] F. Szmulowicz, Solution to spurious bands and spurious real solutions in the envelope-function approximation, Phys. Rev. B, 71, 245117, 2005.
[86] I.V. Tokatly, A.G. Tsibizov, and A.A. Gorbatsevich, Interface electronic states and boundary conditions for envelope functions, Phys. Rev. B, 65, 165328, 2002.
[87] R. G. Veprek, S. Steiger, and B. Witzigmann, Ellipticity and the spurious solution problem of $k \cdot p$ envelope equations, Phys. Rev. B, 76 (16), 165320, 2007.
[88] I. Vurgaftman, J.R. Meyer and L.R. Ram-Mohan Band parameters for III-V compound semiconductors and their alloys Journal of Applied Physics, 89, 5815, 2001.
[89] L.-W. Wang, Real and spurious solutions of the 8x8 $k \cdot p$ model for nanostructures, Phys. Rev. B, 61, 7241, 2000.
[90] L.X. Wang, R. Melnik, Dynamics of shape memory alloys patches with mechanically induced transformations, Discrete and Continuous Dynamical Systems, 15 (4), 1237-1252, 2006.
[91] L.X. Wang, R.V.N. Melnik, Differential-algebraic approach to coupled problems of dynamic thermoelasticity, Applied Mathematics and Mechanics, 27 (9), 1185-1196, 2006.
[92] L.X. Wang, R.V.N. Melnik, Finite volume analysis of nonlinear thermo-mechanical dynamics of shape memory alloys, Heat and Mass Transfer, 43 (6), 535-546, 2007.
[93] L.X. Wang, R.V.N. Melnik, Model reduction applied to square to rectangular martensitic

transformations using proper orthogonal decomposition, Applied Numerical Mathematics, 57 (5-7), 510-520, 2007.

[94] L.X. Wang, R.V.N. Melnik, Simulation of phase combinations in shape memory alloys patches by hybrid optimization methods, Applied Numerical Mathematics, 58 (4), 511-524, 2008.

[95] L.W. Wang, A. Zunger, Linear combination of bulk bands method for large-scale electronic structure calculations on strained nanostructures, Phys. Rev. B, 59 (24), 15806-15818, 1999.

[96] B. Wen, R. Melnik, Relative stability of nanosized wurtzite and graphitic ZnO from density functional theory, Chemical Physics Letters, 466 (1-3), 84-87, 2008.

[97] B. Wen, R.V.N. Melnik, First principles molecular dynamics study of CdS nanostructure temperature-dependent phase stability, Applied Physics Letters, 92 (26), 261911, 2008.

[98] S. R. White and L. J. Sham, Electronic properties of flat-band semiconductor heterostructures, Physical Review Letters, 47, 879, 1981.

[99] M. Willatzen et al., Finite element analysis of nanowire superlattice structures, Computational Science and Its Applications - ICCSA 2003, Pt 2, Proceedings, Lecture Notes in Computer Science, Vol. 2668, 755-763, 2003.

[100] M. Willatzen, R. V. N. Melnik, C. Galeriu, and L. C. Lew Yan Voon Quantum confinement phenomena in nanowire superlattice structures, Mathematics and Computers in Simulation, 65 (4-5), 385-397, 2004.

[101] M. Willatzen, B. Lassen, L.C. Lew Yan Voon, and R.V.N Melnik, Dynamic coupling of piezoelectric effects, spontaneous polarization, and strain in lattice-mismatched semiconductor quantum-well heterostructures, Journal of Applied Physics, 100, 024302, 2006.

[102] R. Winkler and U. Rössler. General approach to the envelope-function approximation based on a quadrature method. Phys. Rev. B, 48, 8918, 1993.

[103] S.H. Xiang, W.H. Gui, and P.H. Mo, Numerical quadrature for Bessel transformations, Applied Numerical Mathematics, 58 (9), 1247-1261, 2008.

[104] W. Yang and K. Chang. Origin and elimination of spurious solutions of the eight-band k·p theory. Phys. Rev. B, 72, 233309, 2005.

[105] K.N. Zotsenko and R.V.N. Melnik, Optimal minimax algorithm for integrating fast oscillatory functions in two dimensions, Engineering Computations, 21 (7-8), 834-847, 2004.